E138 - Institute of Solid State Physics
Vienna University of Technology
Wiedner Hauptstraße 8-10, 1040, Vienna

Infrared studies on antiferroelectric candidate francisite $Cu_3Bi(SeO_3)_2O_2Cl$

Bachelor Thesis of

Malysheva Elena

under supervision of

Univ.Prof. Dr. Andrei Pimenov

Dr. Evan Constable

Dipl.-Ing. Lorenz Bergen

July 2018

Contents

1. Introduction

This thesis focuses on the infrared spectroscopic study of single crystal francisite $Cu_3Bi(SeO_3)_2O_2Cl$ at room temperature. Francisite is a candidate material for supporting a novel antiferroelectic phase characterized by two opposing polar sublattices at low temperatures. It is thought that a characteristic signature of this phase transition is the softening of a low frequency polar phonon mode. While initial phonon characterisations were carried out by Miller *et al*. in reference [1], no soft modes were observed. Experimental optimization for detecting the lowest frequency phonon modes may reveal the presence of the soft modes and thus confirm the antiferroelectic theory. This thesis addresses the preliminary process of optimizing the experiment at room temperature to push the low frequency capabilities.

It also serves as a basis for further investigations aiming at tracking temperature-dependence of reflectance over the range of 300 K – 12 K. The nature of the structural transition occurring at 115 K and accompanying new phonon modes are of a particular interest for condensed matter scientists, as well as the relationship of these two phenomena.

The technique of infrared spectroscopy lends itself well to the investigation of geometrically frustrated magnetic materials, such as francisites. It measures the vibrational energies of molecules. In contrast to absorbance, which is linearly proportional to concentration and mostly used for quantitative analysis, the reflectance spectra correspond to specific vibrational modes and are unique to each molecular structure examined (qualitative analysis) [2].

2. FTIR Hardware

An essential component of the experimental arrangement is a VERTEX 80v (Fig. 2.1) – evacuatable fully digital Fourier-transform infrared spectrometer (FTIR) and the appropriate spectroscopic firmware (OPUS).

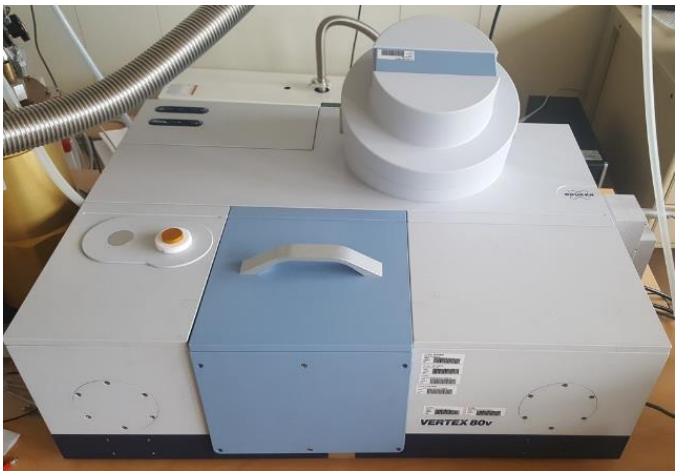

Figure 2.1: Bruker VERTEX 80v.

The spectrometer is equipped with a vacuum pump, allowing measurements to be performed at low pressure (≈ 1 mbar). This effectively removes all substances, especially water vapour, contained in the air that could affect the experimental results. The spectrometer consists of three main components briefly described below.

2.1 Sources

In order to cover the whole frequency range we need to use different light sources.

Apart from the standard mid- and near infrared sources the basic instrument is equipped with, there is also an external far infrared source available. The sources are either air- or water-cooled i.e. their temperature is regulated simply by heat-exchange with the atmosphere or water flow.

2.2 Beam splitters

As the name indicates, a beam splitter splits the incident light beam into two components and then recombines them. The crucial part of each beam splitter is a thin

coating, which has an ability of partly transmit and partly reflect, acting like a semi-transparent mirror.

VERTEX 80v features a default installed KBr beam splitter, optimised for use in the mid-infrared range. In other spectral areas, KBr starts to absorb strongly, thus there is a need in other types of transparent windows. There is a number of optional beam splitters so that in combination with appropriate sources and detectors all infrared spectral ranges can be covered (Tab.1):

	Device	Spectral range [cm^{-1}]	Beam splitter	Detector
VIS/NIR	Halogen lamp	≈ 14000 - 4000	CaF_2	Si-diode
MIR	U-formed silicon carbide stick electrically heated up	≈ 4000 - 400	KBr	MCT
FIR	Mercury-vapor lamp	≈ 400 - 80	Mylar multilayer	silicon bolometer
THz	Mercury-vapor lamp	≈ 80 - 4	Mylar50µm	silicon bolometer

Tab. 1: Light sources in different spectral ranges and their characteristics.

2.3 Detectors

The detector is a devise that responds to an incident radiation flux, turning it into an electrical signal. At the heart of any infrared detector is an element made of a thermally sensitive material. In the range between 400 cm^{-1} and 14000 cm^{-1} this function is performed by a compound called mercury cadmium telluride or MCT for short. The electronic structure of this semi-conductive material has bandgaps with the energy according to the spectral region mentioned above. Thus, the intensity of the incident radiation can be obtained from an electrical signal measured by sensors placed on the surface. After being amplified by the detector`s electronics, the analogue signal is transformed into a digital one and then sent to the computer where a fast Fourier transform (FFT) procedure is performed.

In the longwave-infrared, the MCT is substituted by a *silicon bolometer* (Fig. 2.2).

The main component of the bolometer is a very thin plate made of a semi conductive (Silicon) material and blackened to improve light absorption. It acts as a sensitive thermometer evaluating a temperature increase by a change in the silicon elements resistivity. Thus the beam intensity can be measured.

For optimal performance, the bolometer sensor must be thermally isolated from the laboratory environment. The inclusion in a vacuum reduces external disturbances by heat transfer or convection. An additional Cu-shielding, thermally connected to the nitrogen reservoir at the top is used as a shield against external radiation.

For continuous measurement of the radiant power, the produced heat must to be instantaneous carried away from the thermosensitive element. This is ultimately, what determines the speed at which the moving mirror can be translated in an interferometer as well as the accuracy of the procedure. A thermal link from a heat sink regulates the element's temperature. A high sensitivity is achieved with liquid Helium bolometers, cooled to the temperature lower than 4 K.

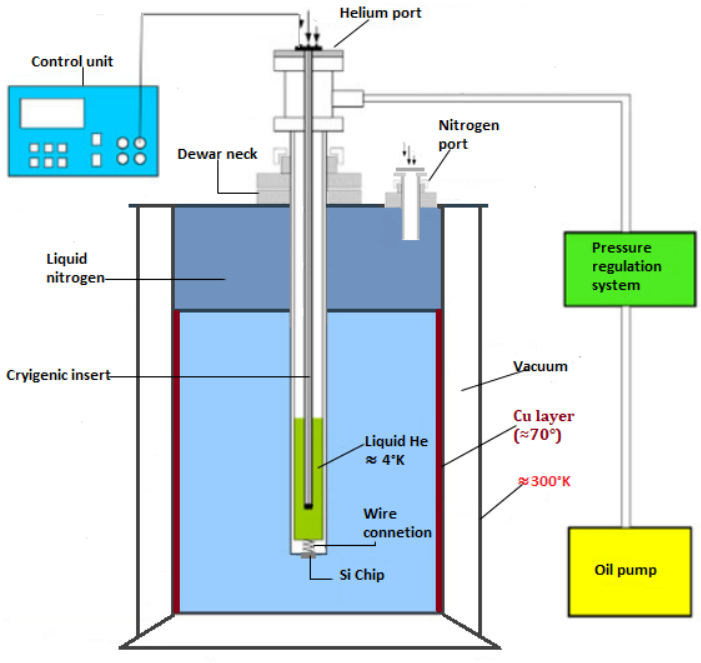

Figure 2.2: Liquid Helium cooled bolometer, image adopted from reference [3].

2.4 Laser

The VERTEX 80v is equipped with a HeNe Laser, which monitors the position of the moving mirror (also called “scanner”). Due to the laser´s high coherence a high precision can be achieved reaching a resolution of +- 0.01 cm^{-1}. This results in a high reproducibility of the consecutive scans.

3. Functional design of FTIR Spectrometer

A Fourier-transform infrared spectrometer (FTIR) is an instrument that measures the reflection or absorbance characteristics of a sample, using computer-assisted Fourier transform. This section is dedicated to a description of the functioning principles of this device. An integral and crucial part of every FTIR is a Michelson interferometer. The optical design (modified with additional devices, in particular a movable mirror and other service functions) is illustrated in Figure 3.1

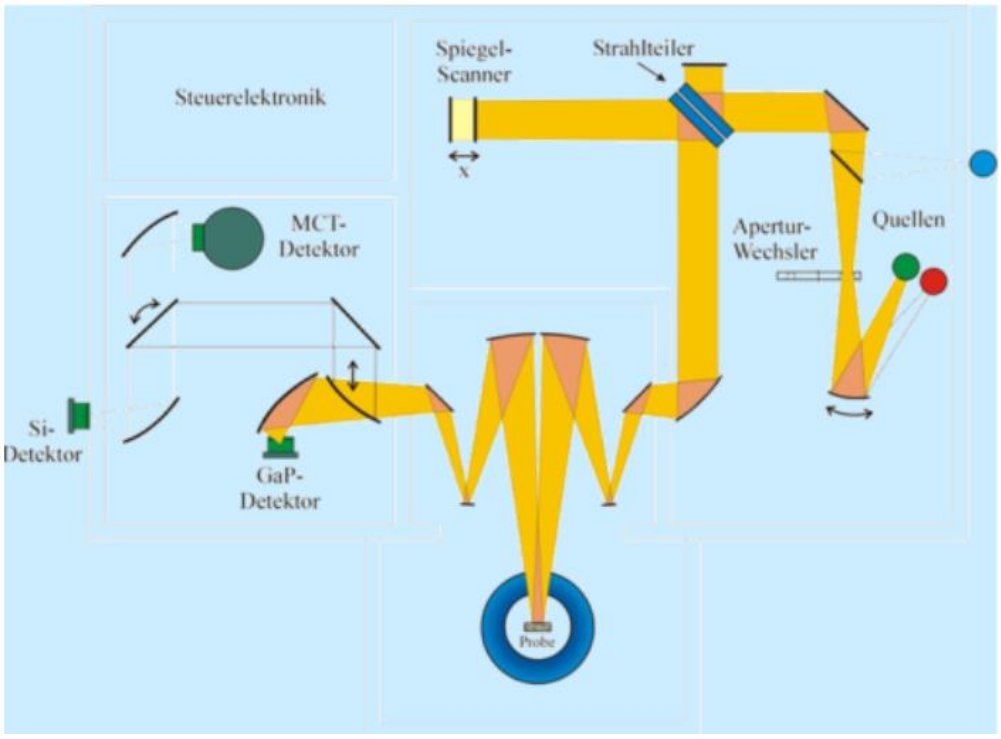

Fig. 3.1: Scheme of the Fourier-Transform Spectrometer, image adopted from reference [4].

It is necessary to describe briefly how the phenomenon of interference produces a spectrum. The light from an infrared source entering the interferometer is directed at the beam splitter, which splits a single light beam into two coherent components causing them to build an interference pattern, once they have been reflected from the fixed and movable mirror and recombined. The movable mirror ensures that the optical path difference between two partial beams can be changed. After interacting with the sample, the detector subsequently measures the intensity of the incident light beam as a function of mirror coordinates. These initial (raw) data are called *interferogram*.

Assuming that the light beam only consists of a single wavelength, the interferogram would feature a trivial sinus wave with alternating maxima and minima depending on the optical path difference regulated by the movable mirror.

An infrared source in a FTIR emits radiation composed of many wavelengths. Different wavelengths are modulated at different rates, which results in an individual intensity composition at each mirror position. Therefore, a real interferogram will have a form as presented in Figure 3.2.

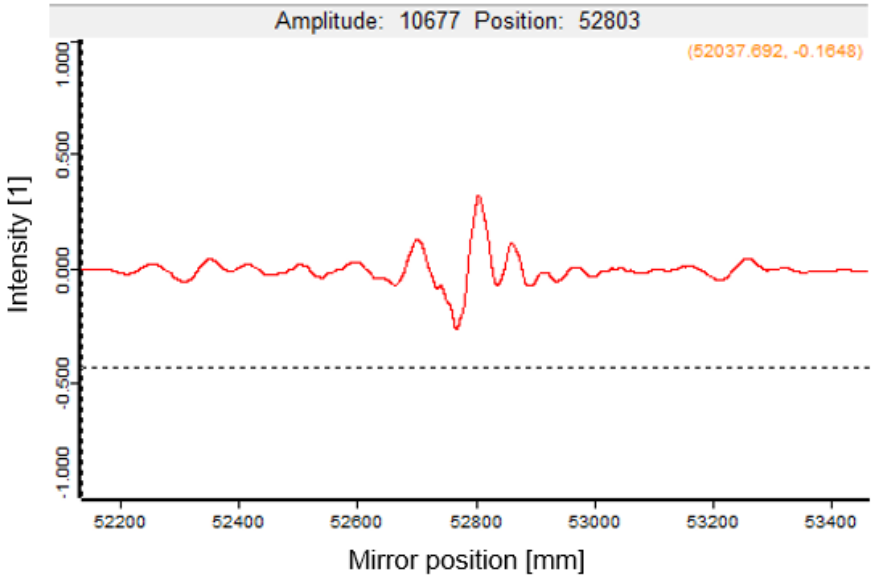

Fig 3.2: FTIR interferogram of a gold mirror reference.

In fact, it is a big advantage of FTIRs that wavelengths over a wide spectral range are measured simultaneously whereas in a dispersive spectrometer, using prisms and dispersive gratings, each component is measured one at a time.

After averaging over the selected number of scans, the actual spectrum (intensity for each wavelength) can be obtained very rapidly by applying Fourier-transformation.

The intensity is measured by the detector as a function of the actual optical path difference p, expressed as [5]:

$$I(p,\tilde{v}\,) = I(\tilde{v})[1+\cos(2\pi p\tilde{v})], \tag{3.1}$$

where $I(\tilde{v})$ is the spectrum to be determined. The total intensity summarized over the complete spectral range is then:

$$I(p) = \frac{1}{\sqrt{2\pi}}\int_0^\infty I(\tilde{v})[1+\cos(2\pi p\tilde{v})]d\tilde{v}. \tag{3.2}$$

Performing an inverse Fourier-Transformation on this relation gives:

$$I(\tilde{v}) = \frac{1}{\sqrt{2\pi}} \int_0^\infty [I(p) - \frac{1}{2} I(p=0)] \cos(2\pi p \tilde{v})\, dp. \quad (3.3)$$

In order to obtain an actual spectrum of sample reflectance it must be compared to the amount of light emitted by the source. For this purpose, we additionally record a gold mirror spectrum, which possess almost 100% reflectance.

4. Measurements

4.1 About the sample

All the measurements in this thesis was carried out on a single-crystal $Cu_3Bi(SeO_3)_2O_2Cl$ also called francisite, a layered material with a frustrated magnetic lattice. At room temperature, the crystal structure features Pmmn space group symmetry and is built up of buckled copper-oxide kagome planes, stacked along the c axis. Below 115 K, francisite undergoes a structural distortion where one mirror plane is connected to a glide plane forming a Pcmn structure described in reference [6]. The distorted structure is shown in Figure 4.1. The lower point group symmetry supports two opposing polar sublattices which makes francisite a strong candidate for antiferroelectric properties [7].

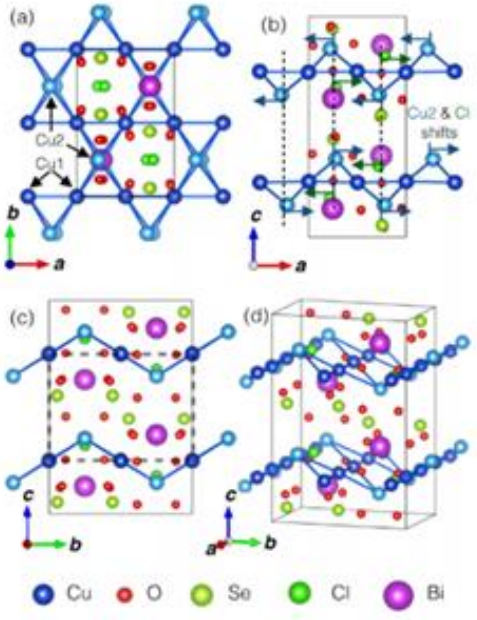

Fig 4.1: ab plane (a), ac plane (b), bc plane (c) and the projected (d) views of the $Cu_3Bi(SeO_3)_2O_2Cl$ crystal structure. The dashed rectangle indicates the high temperature unit cell shown in (c) [7].

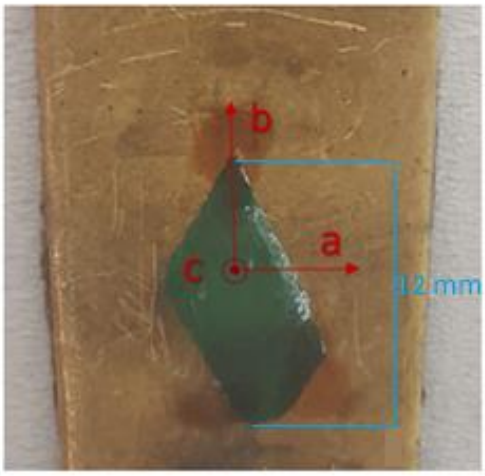

Fig 4.2: Sample with indicated crystallographic axes.

4.2 Measurement procedure

All the measurements were performed at room temperature.

Reference spectra were obtained by reflectance measurements of a gold mirror. The sample reflectivity is determined by a ratio between the sample and reference spectra.

For optimal alignment of the beam at the target (mirror or sample), a re-alignment of the optical system was performed each time after changing to another detector. Recording two equal spectra at each setting respectively and subsequently computing the ratio between them, we can assure the consistency of the measurements.

The anisotropic dielectric properties were probed along a and b axes by using a polarizer transmitting only light polarized in E||a and E||b direction depending on the orientation.

It is vital for every FTIR analysis to maximize the spectral quality. For this purpose, several scanning parameters need to be chosen properly:

- **Resolution and Aperture**

One of the most essential characteristics is the optical resolution, which indicates the ability of a spectrometer to distinguish closely adjoining spectral features.

The resolution is mostly determined by the maximum optical path difference for a scan determined by the moving mirror, as well as by how quick the detector element can respond to changes in the infrared intensity. Both parameters define how many discrete data points are recorded in the interferogram and thus the actual spectrum itself.

In the FTIR used in this experiment, the resolution can be set to different values such as 16 cm^{-1}, 8 cm^{-1}, 4 cm^{-1}, or 2 cm^{-1}.

The resolution can be additionally increased by choosing a smaller aperture (i.e. light beam diameter) but at the expense of signal strength. If the Intensity of the light entering the detector is reduced, the relative amount of noise in the spectra increases proportionally. Therefore, it is undesirable to have a higher than necessary resolution. In the course of the experiment, an optimal combination of both settings was found for each spectral range.

- **Number of scans** simply means how many times the scanning mirror is moved forth and back, essentially, how many separate interferograms are recorded. Due to limited detector sensitivity, the beam intensity measurement at each path difference takes a certain amount of time. More scans are equivalent to an increased observation time, which can significantly reduce the noise level (Signal-to-noise ratio or SNR) in the averaged interferogram.

5. Experiment results and analysis

As said before, the single bounce reflectance spectra was obtained in the experiment for two polarization directions (Figs 5.1 and 5.2).

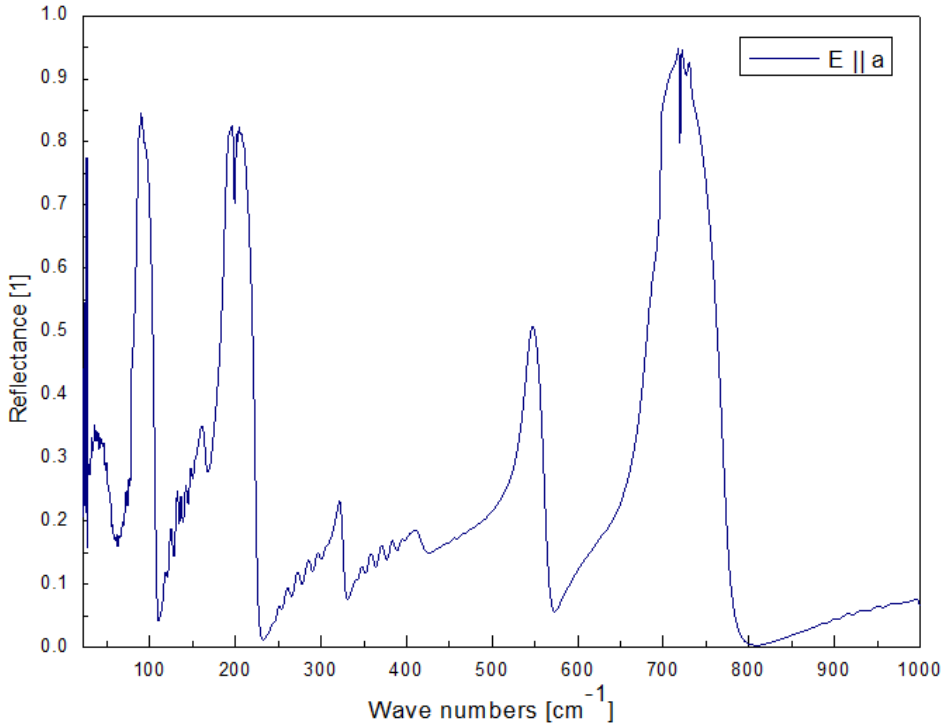

Fig 5.1: Far infrared reflectance spectrum of $Cu_3Bi(SeO_3)_2O_2Cl$ along a-axis.

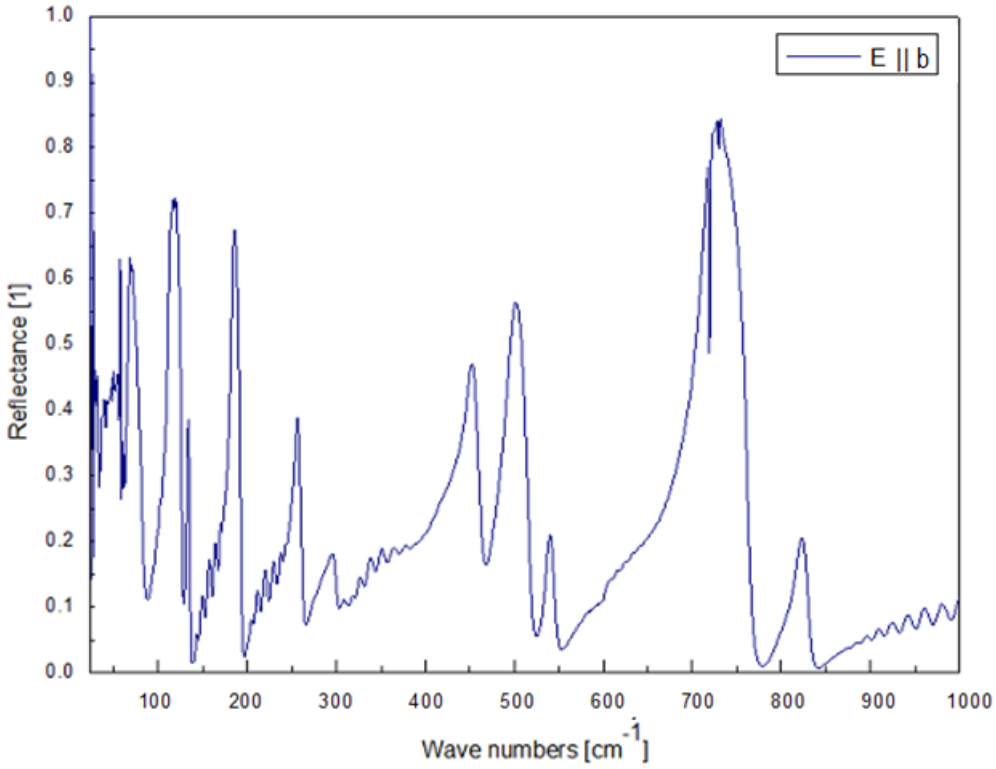

Fig 5.2: Far infrared reflectance spectrum of $Cu_3Bi(SeO_3)_2O_2Cl$ along b-axis.

The resulting spectra can now be compared with those from reference [1] at 300 K (Fig 5.3, black curve). We can see a quite good overlapping of the phonon peaks with them from previous studies, which indicates the consistency of the measurements.

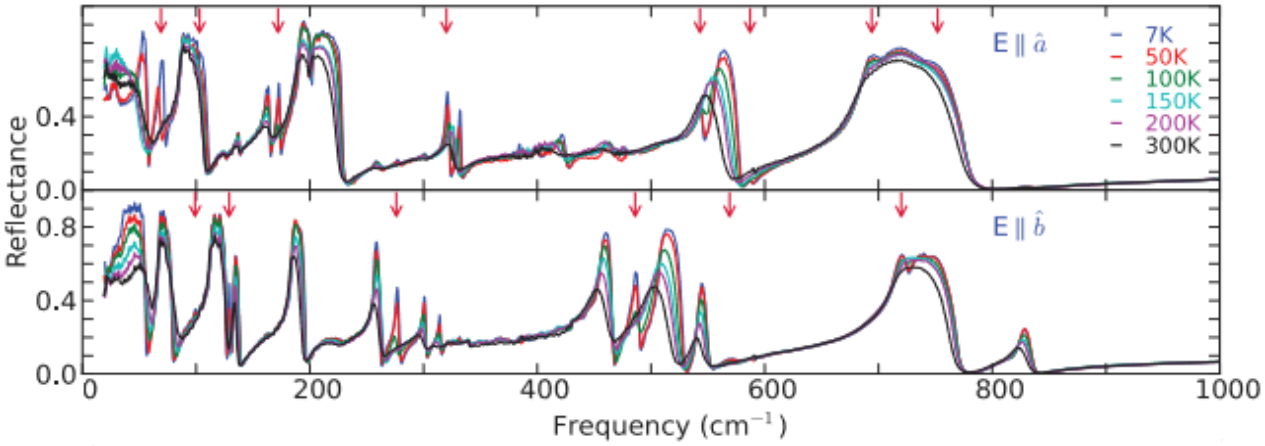

Fig. 5.3: The temperature-dependent reflectance spectra of $Cu_3Bi(SeO_3)_2O_2Cl$ along a and b axes [1].

From Figs. 5.1, and 5.2 one can see clearly visible noise in the range between 0 and 20 cm^{-1}, which refers to an insufficient measurement quality (because of insufficient good signal) and thus no statements regarding the occurrence of phonon modes can be made. However, there is a rather big improvement, starting at approximately 20 cm^{-1}, which allows us to confirm the presence of low lying phonon modes possibly associated with the soft polar phonon that could drive the antiferroelectic phase transition at low temperatures.

The complex dielectric function $\varepsilon(\omega)$:

$$\varepsilon(\omega) = \varepsilon_1(\omega) + i\,\varepsilon_2(\omega), \tag{5.1}$$

reflects the electronic and structural properties of the material. Knowledge of its frequency dependence can help further exploration of the magneto-electric and antiferroelectric properties of the francisites. The real component $\varepsilon_1(\omega)$ describes the phase lag between the driving and response frequency and the imaginary component $\varepsilon_2(\omega)$ is the damping factor showing how the material dissipates electromagnetic energy.

These quantities are not independent of each other and, consequently, there is a principle possibility from the spectrum of one of the optical constants to calculate the spectrum of the other without resorting to direct measurements of the latter. The dielectric constant is directly related to the optical properties. As will be shown below, ε can be easily derived from such optical quantities as refractive index n, and reflection coefficient r. One can take advantage of the fact that the real and imaginary part of

any complex function, analytic in the upper half-plane, are related by the Kramers-Kronig relations. These relations are often used in physics since the analyticity of the response function implies that the system satisfies the causality principle, and vice versa. They imply that observing the dissipative response of a system is sufficient to determine its out of phase (reactive) response, and vice versa. A related goal of the Kramers-Kronig transformation is to find a relation between magnitude and phase of a complex response function [8].

This approach in combination with a knowledge of reflectance R at all frequencies permits one to find the separate values of $\varepsilon_1(\omega)$ and $\varepsilon_2(\omega)$.

In practice, we can measure the reflectance R easily but not its phase. Since R is an analytical function, its amplitude and phase obeys the Kramers-Kronig relations.

As the incident and reflected waves propagate along the same axis, the reflectance R is just the squared magnitude of the reflection coefficient r:

$$R = |r|^2. \tag{5.2}$$

We can also rewrite it as:

$$r = \sqrt{R(\omega)}e^{i\varphi(\omega)}. \tag{5.3}$$

By measuring the $R(\omega)$ - single bounce reflectance, obtained in the experiment, - we utilize the Kramers-Kronig transformation with logarithmic kernel to obtain the reflection phase and, subsequently, the complex reflection coefficient of the sample.

$$\varphi(\omega) = \frac{2\omega}{\pi} v.p. \int_0^\infty \frac{\ln\sqrt{R(\omega')}}{\omega'^2 - \omega^2} d\omega'. \tag{5.4}$$

where $v.p.$ is the abbreviation for the Cauchy principal value of the integral because the denominator in the integrand features a zero. In practice, the calculation can be quite complicated and thus was computer processed in this thesis.

In case of normal incidence the complex Fresnel equation, describing the reflection of light on an interface between different optical media is simplified as follows [9]:

$$r = \frac{n_1 - n_2}{n_1 + n_2}, \tag{5.5}$$

where n complex refractive index: $n_1 = 1$ (vacuum). Transforming this:

$$n_2 = \frac{1-r}{1+r}. \tag{5.6}$$

The relation between the complex refractive index and permittivity in non-magnetic media:

$$n = \sqrt{\varepsilon}\,. \tag{5.6}$$

$$n^2 = (n+ik)^2 = n^2 + 2ink + k^2 = \varepsilon\ = \varepsilon_1 + i\,\varepsilon_2\,. \tag{5.7}$$

Using $R(\omega)$ dependence for the both polarization directions, we utilize the Kramers-Kronig and become the corresponding anisotropic infrared dielectric function tensor components (eps1 is designated as real part $\varepsilon_1(\omega)$, and eps2 as imaginary part $\varepsilon_2(\omega)$ of the electric function).

The graphical representation is seen in Figs. 5.4 (a,b) and 5.5 (a,b) with a zoomed view in the range between 0 and 100 cm^{-1} highlighting the low frequency excitations previously unidentified.

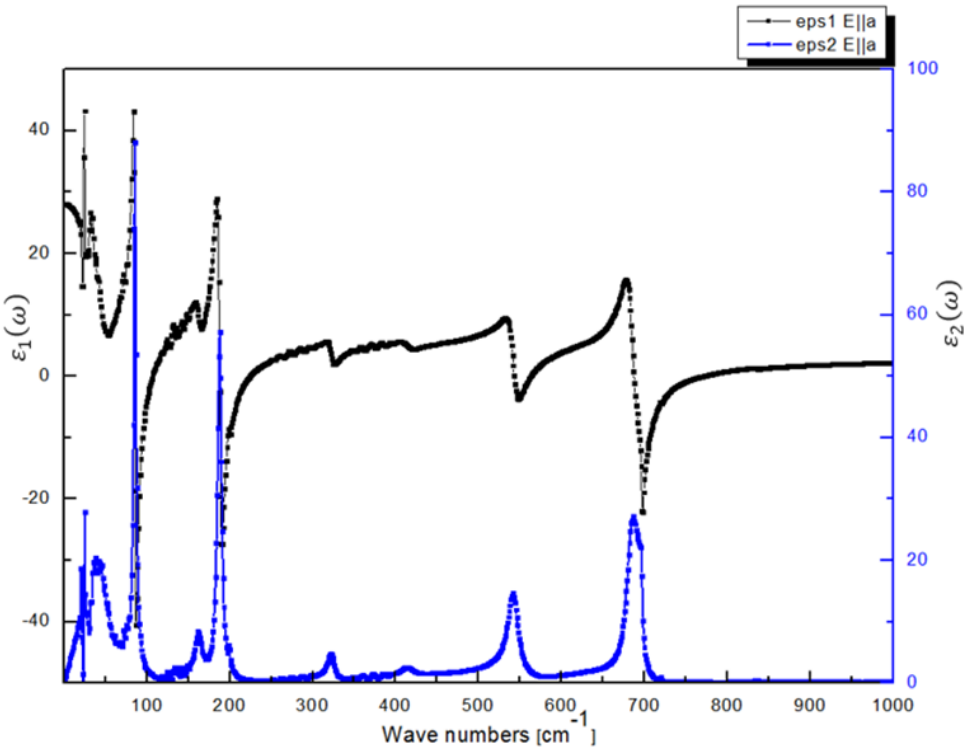

Fig 5.4(a): Eps1 ($\varepsilon_1(\omega)$) and eps2 ($\varepsilon_2(\omega)$) for $Cu_3Bi(SeO_3)_2O_2Cl$ along a axis.

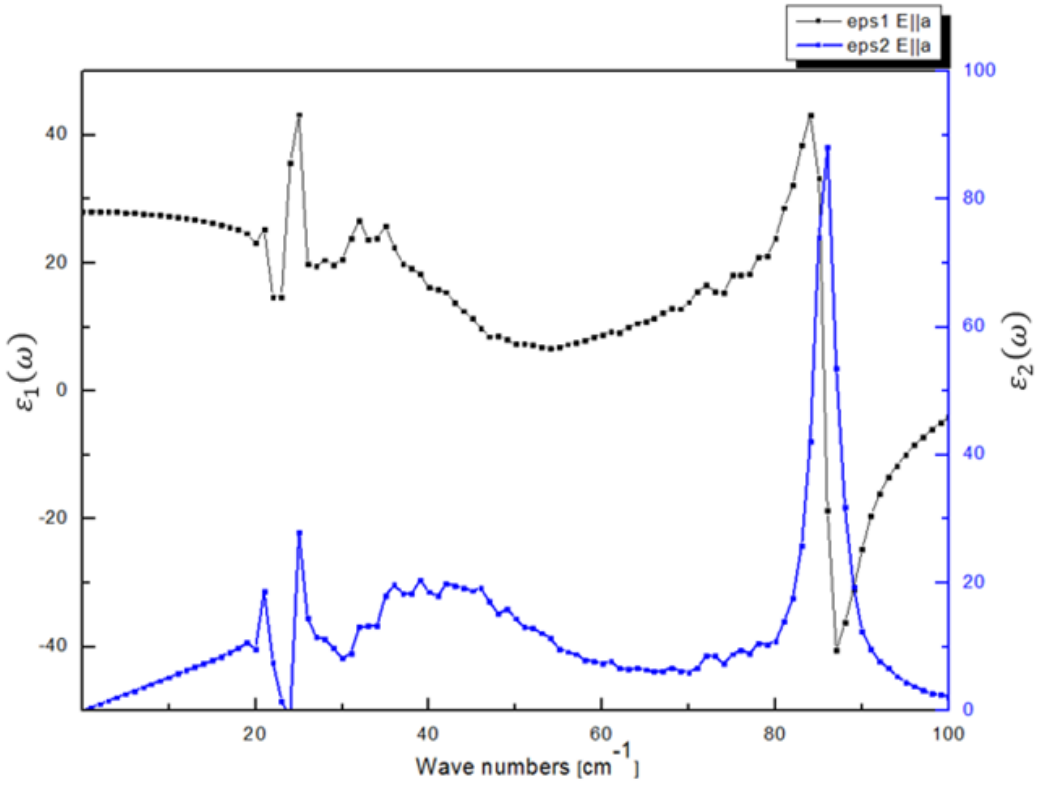

Fig 5.4(b): Zoomed view of eps1 ($\varepsilon_1(\omega)$) and eps2 ($\varepsilon_2(\omega)$) for $Cu_3Bi(SeO_3)_2O_2Cl$ along a axis.

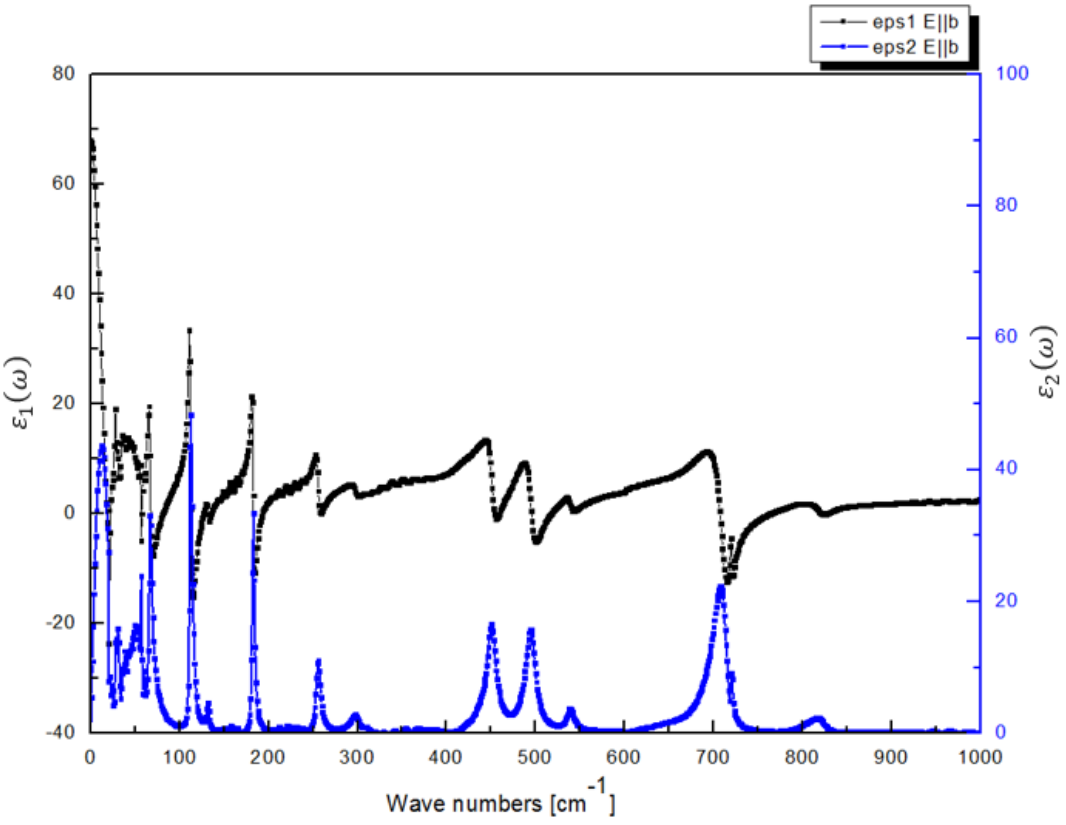

Fig 5.5(a): Eps1 ($\varepsilon_1(\omega)$) and eps2 ($\varepsilon_2(\omega)$) for $Cu_3Bi(SeO_3)_2O_2Cl$ along a axis.

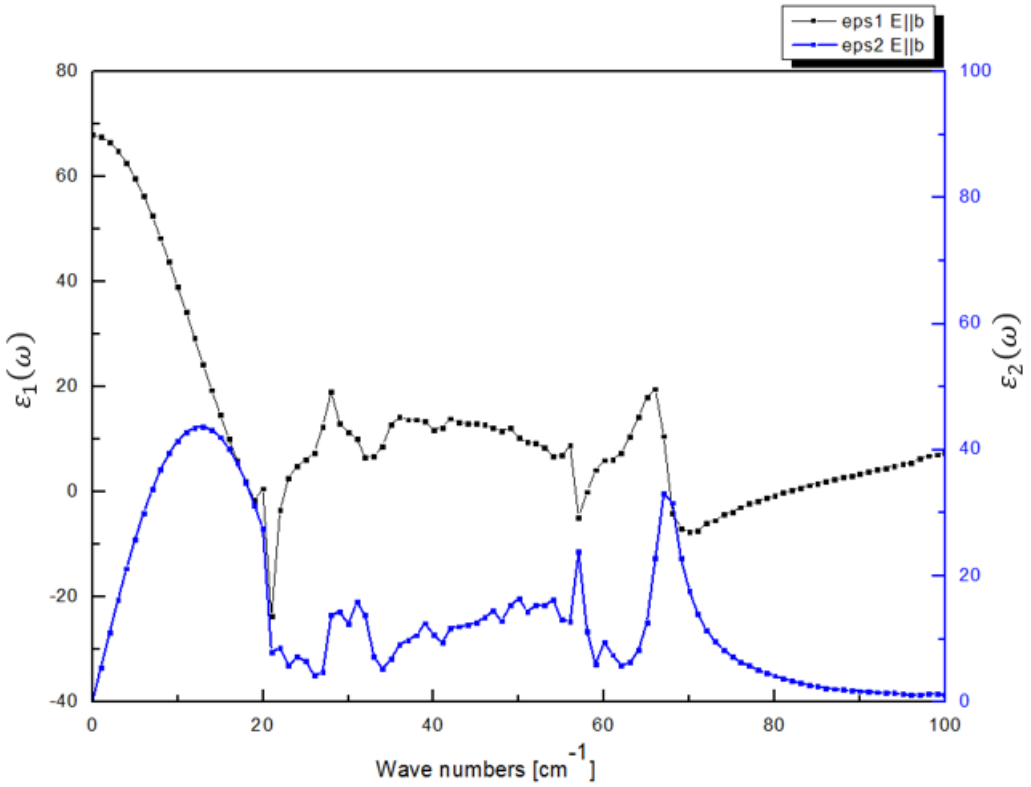

Fig 5.5(b): Zoomed view of eps1 ($\varepsilon_1(\omega)$) and eps2 ($\varepsilon_2(\omega)$) for $Cu_3Bi(SeO_3)_2O_2Cl$ along b axis.

Observing the peaks in the imaginary part of the dielectric function, which describes the phonon response, we can identify the corresponding optical phonon frequencies. With an integrated cursor-function in the Origin Lab Software the numerical values of the peaks can be easily identified (Table 2).

E||a		E||b	
$\tilde{\nu}$ [cm^{-1}]	ε'' [1]	$\tilde{\nu}$ [cm^{-1}]	ε'' [1]
25	28	28	15
36	20	57	24
86	88	67	32
162	9	133	52
189	58	183	33
322	5	255	11
542	15	450	17
687	27	494	16
		707	22

Table 2: Numerical values of phonon peaks for E||a and E||b, beginning at 20 cm^{-1}.

The phonon peaks appearing at 25 cm^{-1}, 36 cm^{-1} and 28 cm^{-1}, 57 cm^{-1} respectively are previously unidentified. They are of a particular interest since they can be associated with previously unexplored phenomena arising in this spectral range. For example, the paraelectric/antiferroelectric phase transition described earlier.

When the sample is aligned along one direction, we maximise some of the phonon excitations. After rotating it by 90°, we observe a completely different spectrum. This confirms the optical anisotropy of the polar crystal, where the ionic motions determine the response function.

6. Summary and Outlook

Reflectance spectra on a single-crystal of fransicite $Cu_3Bi(SeO_3)_2O_2Cl$ were obtained in the spectral range between 15 and 14000 cm^{-1} by using the Fourier-transform infrared spectroscopy (FTIR), whereas the values in the mid- and near infrared were only collected to enable the Kramers-Kronig analysis.

Optical properties of fransicites extracted from the Kramers-Kronig analysis in the longwave-infrared are of a particular interest, since they can be associated with previously unexplored phenomena occurring in these newly discovered compounds. As it was presented in the survey of Miller *et al*. [1], there is a structural phase transition between 110 K and 120 K, followed by appearance of new phonon modes. It would be interesting to confirm these results as well as track the newly identified lowest energy phonon modes as they soften through the phase transition.

This would confirm principal theories for antiferroelectric transitions that incorporate soft polar modes associated to the distortion.

For this purpose, additional measurement at low temperatures would have to be performed in a cryostat. In particular, there is also the possibility to probe the excitations of the magnetic phase below 25 K and how they interact with the lattice degrees of freedom.

7. References

[1] K. H. Miller, P. W. Stephens, C. Martin, E. Constable, R. A. Lewis, H. Berger, G. L. Carr, and D. B. Tanner, “Infrared phonon anomaly and magnetic excitations in single-crystal $Cu_3Bi(SeO_3)_2O_2Cl$”. Phys. Rev. B 86, 174104 (2012).

[2] B. C. Smith, “Fundamentals of Fourier Transform Infrared Spectroscopy”, CRC Press, 2011.

[3] Picture updated from http://www.infraredlaboratories.com,
Url: <http://www.infraredlaboratories.com/Bolometers.shtml>

[4] Picture updated from TU Wien, Solid State Spectroscopy Group.
Url: <https://www.ifp.tuwien.ac.at/spectroscopy/research/>

[5] Wikipedia: Fourier-transform spectroscopy,
Url: <https://en.wikipedia.org/wiki/Fourier-transform_spectroscopy>

[6] E. Constable, S. Raymond, S. Petit, E. Ressouche, F. Bourdarot, J. Debray, M. Josse, O. Fabelo, H. Berger, S. deBrion and V. Simonet, “Magnetic and dielectric order in the kagomelike francisite $Cu_3Bi(SeO_3)_2O_2Cl$” Phys. Rev. B 86, 174104 (2012).

[7] P. Tolédano, M.Guennou, “Theory of antiferroelectric phase transitions”, Phys. Rev. B 86, 174104 (2012).

[8] Michael F. Modest, “Radiative Heat Transfer”, chapter “Optical properties of solids“, 2nd ed. Boston, MA: Academic, 2003.
Url: <https://ocw.mit.edu/courses/mechanical-engineering/2-58j-radiative-transfer-spring-2006/readings/>

[9] Prof. Dr. Helmut Föll, Lectures “Advanced Materials B“. Institute for Material Science of University of Kiel.
Url: <https://www.tf.unikiel.de/matwis/amat/admat_en/>